Applied Physics Letters

# Continuous real-time detection of quasiparticle trapping in aluminum nanobridge Josephson junctions

Cite as: Appl. Phys. Lett. **119**, 122601 (2021); https://doi.org/10.1063/5.0063445
Submitted: 14 July 2021 • Accepted: 06 September 2021 • Published Online: 24 September 2021

J. T. Farmer, A. Zarassi, D. M. Hartsell, et al.

# Continuous real-time detection of quasiparticle trapping in aluminum nanobridge Josephson junctions

Cite as: Appl. Phys. Lett. **119**, 122601 (2021); doi: 10.1063/5.0063445
Submitted: 14 July 2021 · Accepted: 6 September 2021 ·
Published Online: 24 September 2021

View Online Export Citation CrossMark

J. T. Farmer,[1,2] A. Zarassi,[1,2] D. M. Hartsell,[1,2] E. Vlachos,[1,2] H. Zhang,[2,3] and E. M. Levenson-Falk[1,2,a)]

## AFFILIATIONS

[1]Department of Physics and Astronomy, Dornsife College of Letters, Arts, and Sciences, University of Southern California, Los Angeles, California 90089, USA
[2]Center for Quantum Information Science and Technology, University of Southern California, Los Angeles, California 90089, USA
[3]Department of Electrical Engineering, Viterbi School of Engineering, University of Southern California, Los Angeles, California 90089, USA

[a)]Author to whom correspondence should be addressed: elevenso@usc.edu

## ABSTRACT

Nonequilibrium quasiparticles are ubiquitous in superconducting electronics. These quasiparticles can trap in the internal Andreev bound states of a phase-biased Josephson junction, providing a mechanism for studying their presence and behavior. We characterize a quasiparticle trapping detector device based on a two junction aluminum nanobridge superconducting quantum interference device incorporated into a transmission line resonator. When the device is flux-biased, distinct resonant frequencies develop depending on the trapped quasiparticle number. We demonstrate continuous detection of up to 3 trapped quasiparticles, with detection of a trapped quasiparticle with a signal-to-noise ratio of 27 in 5 $\mu$s. We describe initial measurements of quasiparticle behavior and discuss the possible optimization and application of such detector devices.



Superconducting qubits and other low-temperature superconducting electronics have ubiquitous populations of quasiparticles (QPs) far above their thermal equilibrium prevalence.[1–7] These QPs can cause loss,[8] spurious excitation,[9] and spectral noise when tunneling across qubit junctions. Even when QP populations are extraordinarily low,[10] rare bursts of QPs can induce correlated errors that are difficult to address with error correction algorithms.[11,12] QPs may be generated by stray infrared photons,[13] cosmic rays and other high-energy radiation sources,[11,12,14,15] or materials defects.[16] Many experiments have probed QP behavior via their tunneling across Josephson junctions in charge-sensitive transmons,[9,17–19] giving valuable insight into their effects on qubits. However, these measurements are discrete and cannot distinguish between 0 and 2 tunneling events. Trapping measurements[20–24] provide a tool for continuous, nonsaturating monitoring of QP behavior. Furthermore, QP traps have been proposed as a tool to mitigate QPs' effects on qubits,[5,17,25,26] as QPs may diffuse great distances after being generated.[12,15,27] The trapping process itself is, thus, worthy of study, in addition to providing insight into bulk QP behavior.

In this Letter, we characterize a device optimized for continuous, non-saturating measurements of QP trapping in Andreev states. Using microwave reflectometry, we are able to continuously detect 0, 1, and 2 or more trapped quasiparticles in 5 $\mu$s with a signal-to-noise ratio (SNR) of 27. By altering the detector bias, we are also able to distinguish 3, 2, and 1 or fewer QPs. We discuss straightforward improvements that can further improve SNR and allow detection of many more trapped QPs at a single bias point. Our device provides a prototype for detectors optimized for continuous measurements of QP behavior and properties and for studies of the dynamics of Andreev states coupled to resonant cavities.

In the semiconductor picture of the Josephson effect, supercurrent is carried by electrons/holes traveling in 1 dimensional conduction channels. At the junction boundaries, the electron (hole) reflects as a hole (electron).[28] This Andreev reflection causes a $\pm 2e$ charge transfer, where $e$ is the elementary charge, and, thus, transmits a Cooper pair across the junction. Each channel forms a pair of Andreev bound states with energies

$$E_{A\pm} = \pm\Delta\sqrt{1-\tau\sin^2\frac{\delta}{2}}, \tag{1}$$

where $\Delta$ is the superconducting gap, $\tau$ is the transmittivity of the channel, and $\delta$ is the phase bias across the junction. In the semiconductor picture, the Fermi energy is 0, so at temperatures $T \ll \Delta/k_B$, normally the upper Andreev state is unoccupied and the lower state is occupied, carrying the supercurrent across the junction. This is the channel's $|g\rangle$ state with total energy $-E_A$. QPs in the bulk only exist at energies greater than $\Delta$ (or as unoccupied states below $-\Delta$), so it is energetically favorable for a QP to drop into the unoccupied upper Andreev state, bringing the channel to the $|o\rangle$ state with 0 energy. This "poisons" the channel, eliminating it from carrying supercurrent and increasing the Josephson inductance. The lower-level QP may also be promoted to the upper Andreev level, bringing the channel to the $|e\rangle$ and producing twice the inductance shift of the $|o\rangle$ state; or this QP may be cleared from the junction completely, creating another degenerate 0-energy $|o\rangle$ state with 0 supercurrent (see the supplementary material). Researchers have demonstrated continuous monitoring of QPs' trapping in point contact[22] and semiconductor nanowire[23,24] junctions; however, these junctions have few channels and so quickly saturate as QP detectors.

Three dimensional aluminum nanobridge Josephson junctions achieve good phase confinement and nonlinearity in an all-superconducting design.[29–31] Importantly, nanobridges comprise many conduction channels ($\sim$100–1000) with $\tau \sim 1$, approximately following the Dorokhov distribution $\rho(\tau) = \frac{\pi\hbar G}{2e^2}\frac{1}{\tau\sqrt{1-\tau}}$, where $G$ is the junction's normal-state conductance.[32] When 2 identical nanobridges are placed in a loop, forming a superconducting quantum interference device (SQUID), the junctions' phase bias $\delta$ is simply set by the flux bias $\Phi$ as $\delta = \pi\phi$, where $\phi \equiv \Phi/\Phi_0$ and $\Phi_0$ is the flux quantum. In an Al nanobridge SQUID near half-flux ($\delta \approx \pi/2$), a channel with $\tau \approx 1$ has $E_{A+}/h \approx 29$ GHz, or a trap depth of $(\Delta - E_A)/h \approx 12$ GHz, far greater than the thermal energy at 15 mK. These junctions, thus, function as QP traps with many deep trap states when they are phase-biased.

Our device consists of a co-planar waveguide (CPW) resonator in which the center trace is terminated by a nanobridge SQUID; see Figs. 1(a) and 1(b). Fabrication details are given in the supplementary material. The fundamental (quarter-wavelength) mode of our resonator with zero flux through the SQUID is at $\omega_0(0) = 2\pi \times 4.302$ GHz and has linewidth $\kappa = 2\pi \times 250$ kHz, largely set by the coupling to the microwave feedline. This device was imaged and found to have junctions that appear nearly identical visually; past studies indicate that they may, thus, be treated as symmetric.[30,31] Trapping in either junction produces a similar resonant frequency shift, and so, for QP detector applications, they may be thought of as a single junction with twice the number of channels. We note that the resonator energy per photon is much smaller than the trap depth at high flux bias, so absorption of resonator photons should not appreciably affect the quasiparticle states (see the supplementary material).

Our measurement setup is shown schematically in Fig. 1(c). A signal generator provides a drive tone at $\omega_d(\phi) \approx \omega_0(\phi) - \kappa/2$. A power splitter sends half of this power into the dilution refrigerator where it is attenuated then (in some cooldowns) filtered by K&L 12 GHz and Eccosorb low-pass filters. The drive tone is circulated to reflect off our device, which is flux tunable via a DC coil in the packaging, and amplified by a traveling wave parametric amplifier[33]

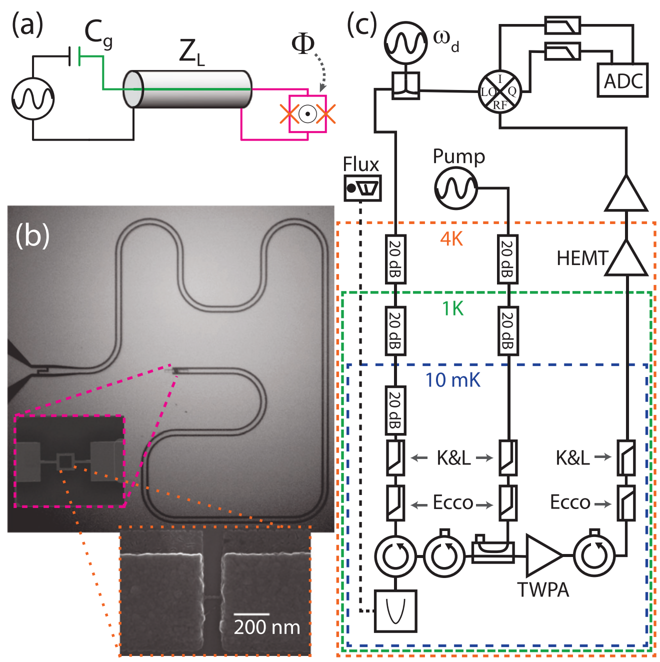


**FIG. 1.** (a) Device schematic. A CPW resonator (green) is grounded via a two-junction Al nanobridge SQUID (magenta). Flux bias through the SQUID phase-biases the junctions as $\delta = \pi\phi$. (b) Optical image of the device with inset SEM images of the SQUID (magenta) and a nanobridge junction (orange). (c) Simplified measurement schematic. A tone at $\omega_d$ continuously drives the flux-tunable resonator. The reflected signal is amplified by a TWPA at base stage followed by a HEMT at 4 K and room temperature amplifiers. Isolators between HEMT and room temperature amplifiers are not shown to conserve space. The amplified signal is homodyne demodulated, and I and Q components are low-pass filtered at 15 MHz, then digitized by an Alazar ATS9371 at 300 MSa/s, and down-sampled to 10 MSa/s before saving. Microwave lines are optionally filtered at base stage by K&L 12 GHz and custom Eccosorb 110 low-pass filters.

(TWPA), which is pumped at 8.078 GHz. The reflected signal is further amplified before IQ demodulation with reference to the original signal. The in-phase (I) and quadrature (Q) components are 15 MHz low-pass filtered before digitization at 300 MSa/s. Raw data are down-sampled to 10 MSa/s before saving.

We first characterize our device with ensemble-averaged vector network analyzer (VNA) measurements of the resonance. Figure 2(a) shows resonance measurements at flux biases of $\phi = 0$ and $\phi = 0.49$, taken on a cooldown in which the K&L and Eccosorb filters were removed. The $\phi = 0.49$ trace in orange shows two shallow peaks at $\sim$0.5 and 1 MHz below the main resonance. These are the resonance peaks with 1 and 2 trapped QPs, respectively, showing the resonance shifting due to the change in nanobridge inductance. These ensemble measurements average over all possible QP trapping configurations, and so a resonance peak amplitude corresponds to the probability of that configuration. We then move on to time-domain IQ measurements as described above. Panels (b) and (c) are log-scale histograms showing 30 s of continuous IQ data for $\phi = 0$ (in blue) and $\phi = 0.47$ (in orange), respectively. The data shown has been integrated by convolving with a Gaussian window of effective integration time $\sqrt{2\pi}\sigma = 3\ \mu$s. In the finite-flux data of panel (c), we can immediately see

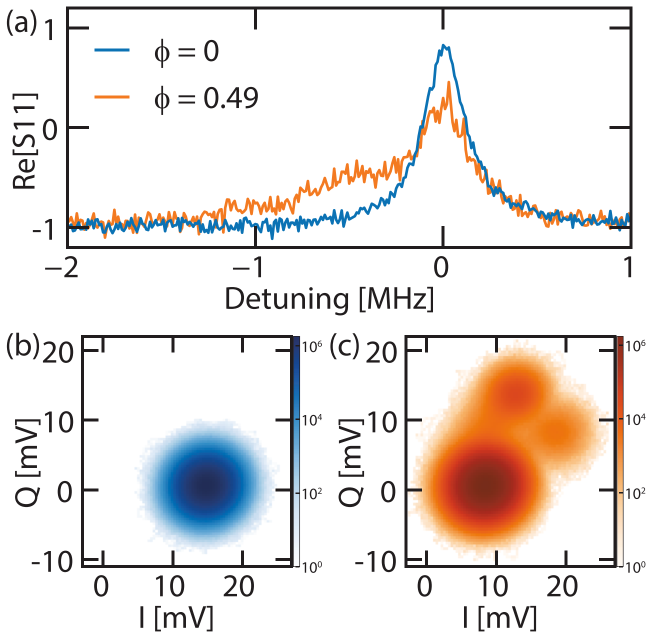


FIG. 2. (a) Ensemble measurement of resonator response at 0 flux (blue) and at $\phi = 0.49$ (orange). When $\phi = 0.49$, distinct peaks are visible roughly 0.5 and 1 MHz below resonance, corresponding to 1 and 2 trapped QPs, respectively. (b) Histogram of continuous IQ data taken at 0 flux for 30 s. Data have a 10 MHz sample rate and have been convolved with a Gaussian window with effective integration time of 3 $\mu$s. (c) Data taken at $\phi = 0.47$ with the same procedure as panel b. The darkest mode is due to the resonance with 0 trapped QPs. The second darkest, located near (I,Q) = (12, 15 mV), corresponds to 1 trapped QP, and the last mode corresponds to 2 or more trapped QPs (as this mode corresponds to the resonance moving far from the drive frequency).

three distinct modes with excellent separation in the log scale plots. The darkest peak (lower left), with the most counts by far, is due to the response with 0 QPs in Andreev traps. The next darkest (upper center) is from having 1 QP trapped, while the lightest mode (middle right) is from 2 QPs in Andreev traps and/or excitation of a single channel into the $|e\rangle$ state. Trapping of more than 2 QPs moves the resonance multiple linewidths and, thus, saturates the change in response to additional trapping, so these counts lie on top of the 2-QP distribution. We later discuss methods for avoiding this saturation. By probing at a frequency close to the 2-QP resonant frequency, we are able to observe 0, 1, 2, and 3 QP modes, confirming that we do indeed see multiple QPs' trapping and not simply the $|e\rangle$ state of a single channel; data are shown in the supplementary material. We have verified that these modes are indeed due to Andreev trapping of QPs by measuring the weights of each mode in the presence of a "clearing tone" at 17 GHz. A trapped QP may absorb a photon from this tone and so be promoted back into the bulk continuum; the frequency was chosen to be greater than the trap depth and because it happens to couple efficiently into the device. We find that the tone causes the 1- and 2-QP mode counts decrease, while the 0-QP mode counts increase. We have also observed that both the separations and the weights of the modes increase as a function of flux, which agrees qualitatively with a QP trapping picture (see the supplementary material).

We now turn to extracting the QP trap occupation as a function of time from the continuous IQ data. To optimize our analysis procedures, we choose data that stress the detector's capabilities. We use data from a cooldown with the K&L and Eccosorb filters, which reduces QP generation by infrared radiation and, thus, shows a much lower QP number than that shown in Fig. 2,[9] and use a low resonator drive power chosen to ensure that the drive does not affect the QP configuration (see the supplementary material). We increase the integration time to 5 $\mu$s to compensate for this loss of SNR. We first fit histograms using a Gaussian mixture expectation–maximization algorithm implemented by the Python module available from scikit-learn.[34] This module takes in a subset of data, assigns each point to one of the specified number of modes, and then tweaks assignments and mode parameters to maximize the total likelihood for all data and all modes. The result is a set of 3 Gaussian modes describing the data, shown by their 1-$\sigma$ (solid) and 2-$\sigma$ (dashed) contours overlaying the histogram in Fig. 3(a). We, then, assign each time-series point to the mode with the highest posterior probability after Bayesian updating with a three-sample rolling memory window to update the prior (see the supplementary material). Unfortunately, the Gaussian mixture fit is unreliable in terms of quality of fit and reproducibility of Gaussian mode parameters, which can vary significantly even when refitting the same data with the same initial guess. This unreliability is apparent from the fit distributions shown, which do not faithfully represent the means of the 1- and 2-QP modes.

To improve the fits, we need to "initialize" the trapped QP configuration, thereby isolating each Gaussian mode for independent fitting. This is challenging, as we have no direct control of the trapped QP number. Fortunately, the Gaussian mixture procedure assigns most data points to the correct occupation. We use this initial assignment to fit the mean lifetime of each mode $\langle\tau_i\rangle$ and, then, identify periods in the time series when the extracted QP occupation is stationary for at least $4\langle\tau_i\rangle$. By stitching these "quiet periods" together, we build up large distributions of data points that are pre-assigned to modes. Each distribution is then independently fit to a Gaussian to fix its mean and covariance. Finally, the full dataset is fit to a mixture of 3 Gaussians with these same means and covariances, with the weight of each mode as the only free parameters. Figure 3(b) shows the result, with 1-$\sigma$ (solid) and 2-$\sigma$ (dashed) contours overlaying the data histogram. It is immediately evident that the quiet periods method produces a better quality of fit.

We extract QP occupation from time series as before with updated Gaussian parameters. Figure 3(c) shows two 0.5 ms sections of data with a 5 $\mu$s Gaussian convolution. These sections were chosen to demonstrate switching events and are far more "active" than typical data, which mostly stays in the 0 QP mode. The background shading represents the extracted QP trap occupation (light blue for 0 QPs, dark blue for 1, and orange for 2 or more). Transitions between the 3 configurations are clearly visible and appear to be faithfully captured by the assignment algorithm. The detector's SNR at our operating parameters ($\sim$4 photon drive power, 5 $\mu$s integration), defined as the separation of mode centers in the IQ plane squared divided by a product of their standard deviations along the line between them, is 27 for 0–1 distinguishability, 32 for 1–2, and 30 for 0–2. The 0–1 SNR gives a detector noise floor of $6.1 \times 10^{-4}$ QPs/$\sqrt{\text{Hz}}$, i.e., we can detect 0.00061 of the signal from a QP trapping with SNR = 1 after 0.5 s of integration, assuming a stationary occupation.

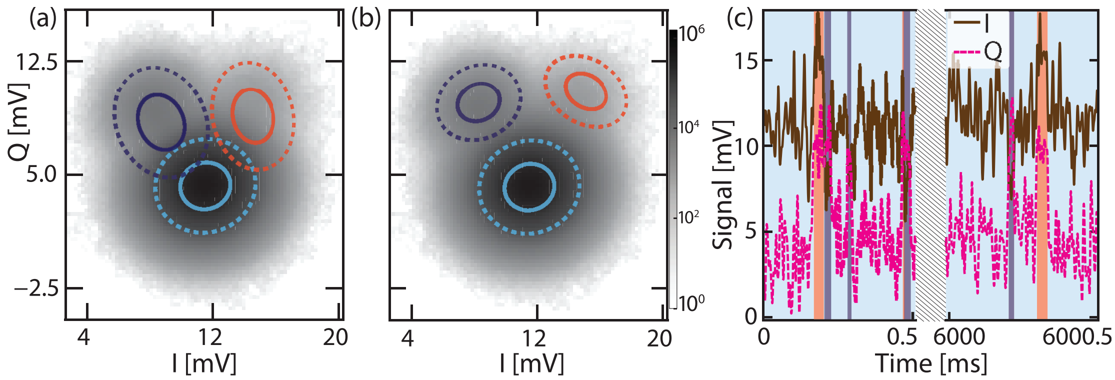


**FIG. 3.** (a) Initial clustering of 5 $\mu$s integrated data using the scikit-learn Gaussian mixture module produces modes with $1\sigma$ (solid) and $2\sigma$ (dashed) contours for 0, 1, and 2 or more trapped QPs in light blue, dark blue, and orange, respectively. (b) Subsets of the data in which the occupation is constant for a long time ($4\langle\tau_i\rangle$) are individually fit to Gaussian distributions. Means and covariances of each mode are then fixed, and the full dataset is fit with mode weights as the only free parameters. (c) Two sections of time series data with I in brown and Q in dashed magenta. The background color is light blue, dark blue, and orange for 0, 1, and 2+ trapped QPs, respectively. All data taken at $\phi = 0.47$.

We now briefly describe the QP behavior measured with our device (see the supplementary material for more detail). We see a mean trap occupation of $n_{qp} = 0.0185$, state occupation probabilities of $P_0 = 0.983$, $P_1 = 0.0155$, $P_2 = 0.00148$, and state lifetimes of $\tau_0 = 728\,\mu$s, $\tau_1 = 12.7\,\mu$s, $\tau_2 = 4.73\,\mu$s. These lifetimes are corrected for the detector bandwidth assuming Poisson switching processes.[35] The distributions of lifetimes do appear Poissonian in the long-time limit, but better SNR (discussed below) may resolve fast events, which may show non-Poisson behavior. We also note that we see transitions between all three of the 0, 1, and 2 QP modes. We attribute the 0–2 transitions to either correlated trapping of 2 QPs in less than a detector bandwidth or direct $|g\rangle \rightarrow |e\rangle$ excitation of a single channel; spectroscopic measurements of the trapped QPs should be able to distinguish between these processes (see the supplementary material). Future work will probe switching rates as a function of bias and environmental parameters (e.g., flux and temperature), analyze correlations between switching events, and develop more sophisticated state-assignment algorithms that do not assume independent (Poisson) switching.

We note that our device is not fully optimized for high sensitivity. While the resonant frequency was kept low in order to be less than the trap depth, raising the resonance slightly to $\sim$6 GHz by shortening the waveguide would increase the participation ratio of the nanobridge inductance to total inductance while still remaining far below trap-clearing frequencies. Similarly, reducing the resonator's characteristic impedance from 50 $\Omega$ to an easily achievable $\sim$30 $\Omega$ would further reduce the linear inductance, increasing sensitivity. Additionally, the TWPA used as a first-stage amplifier had a moderate $\approx$ 15 dB gain (due to being operated near the edge of its bandwidth) and adds noise above the quantum limit. Adding a standard parametric amplifier with a near-quantum-limited noise temperature and 20 dB of gain as a preamplifier will further improve the SNR. We may also trade off some of this sensitivity and increase the resonator bandwidth, thus allowing for detection of more than 2 QPs without saturating the response. We also note the possibility of detecting higher numbers of trapped QPs by probing the device with multiple probe tones simultaneously. By performing heterodyne measurement of probe tones centered on, e.g., the 1-, 3-, and 5-QP resonant frequencies, and correlating the measured outcomes, we should be able to detect up to 6 trapped QPs with a similar device.

In conclusion, we have developed a device for the ultra-low-noise continuous detection of up to 2 quasiparticles trapping in Andreev bound states. Our device is capable of detecting a trapped QP with a SNR of 27 in 5 $\mu$s, giving it a noise floor of $6.1 \times 10^{-4}$ QPs/$\sqrt{\text{Hz}}$. Straightforward extensions are possible to higher sensitivity and QP saturation number. Our device can be used for QP studies, including statistical analysis of trapping and untrapping rates and trap occupation, spectroscopic measurements of trapped QP energy distributions, effects of environmental variables, such as temperature, and testing of QP mitigation techniques.

See the supplementary material for fabrication details, participation ratio calculations, readout power dependence, methods to extract multiple quasiparticle occupation, and determine their lifetimes.

The authors would like to acknowledge J. Aumentado and L. Glazman for useful discussions. They acknowledge MIT Lincoln Laboratory and IARPA for providing the TWPA used in this work. This work was funded by the AFOSR YIP under Grant No. FA9550-19-1-0060 and by the NSF DMR under Grant No. DMR-1900135.

## DATA AVAILABILITY

The data that support the findings of this study are available from the corresponding author upon reasonable request.

## REFERENCES


[1] J. Aumentado, M. W. Keller, J. M. Martinis, and M. H. Devoret, "Nonequilibrium quasiparticles and 2e periodicity in single-cooper-pair transistors," Phys. Rev. Lett. **92**, 066802 (2004).

[2] J. M. Martinis, M. Ansmann, and J. Aumentado, "Energy decay in superconducting Josephson-junction qubits from nonequilibrium quasiparticle excitations," Phys. Rev. Lett. **103**, 097002 (2009).

[3] G. Catelani, J. Koch, L. Frunzio, R. J. Schoelkopf, M. H. Devoret, and L. I. Glazman, "Quasiparticle relaxation of superconducting qubits in the presence of flux," Phys. Rev. Lett. **106**, 077002 (2011).

[4] D. Rainis and D. Loss, "Majorana qubit decoherence by quasiparticle poisoning," Phys. Rev. B. **85**, 174533 (2012).
[5] C. Wang, Y. Y. Gao, I. M. Pop, U. Vool, C. Axline, T. Brecht, R. W. Heeres, L. Frunzio, M. H. Devoret, G. Catelani, L. I. Glazman, and R. J. Schoelkopf, "Measurement and control of quasiparticle dynamics in a superconducting qubit," Nat. Commun. **5**, 5836 (2014).
[6] U. Vool, I. M. Pop, K. Sliwa, B. Abdo, C. Wang, T. Brecht, Y. Y. Gao, S. Shankar, M. Hatridge, G. Catelani, M. Mirrahimi, L. Frunzio, R. J. Schoelkopf, L. I. Glazman, and M. H. Devoret, "Non-poissonian quantum jumps of a fluxonium qubit due to quasiparticle excitations," Phys. Rev. Lett. **113**, 247001 (2014).
[7] L. Glazman and G. Catelani, "Bogoliubov quasiparticles in superconducting qubits," SciPost Phys. Lect. Notes **31**, 1–40 (2021).
[8] S. Gustavsson, F. Yan, G. Catelani, J. Bylander, A. Kamal, J. Birenbaum, D. Hover, D. Rosenberg, G. Samach, A. P. Sears, S. J. Weber, J. L. Yoder, J. Clarke, A. J. Kerman, F. Yoshihara, Y. Nakamura, T. P. Orlando, and W. D. Oliver, "Suppressing relaxation in superconducting qubits by quasiparticle pumping," Science **354**, 1573–1577 (2016).
[9] K. Serniak, M. Hays, G. De Lange, S. Diamond, S. Shankar, L. D. Burkhart, L. Frunzio, M. Houzet, and M. H. Devoret, "Hot nonequilibrium quasiparticles in transmon qubits," Phys. Rev. Lett. **121**, 157701 (2018).
[10] A. Somoroff, Q. Ficheux, R. A. Mencia, H. Xiong, R. V. Kuzmin, and V. E. Manucharyan, "Millisecond coherence in a superconducting qubit," arXiv:2103.08578 (2021).
[11] A. P. Vepsäläinen, A. H. Karamlou, J. L. Orrell, A. S. Dogra, B. Loer, F. Vasconcelos, D. K. Kim, A. J. Melville, B. M. Niedzielski, J. L. Yoder, S. Gustavsson, J. A. Formaggio, B. A. VanDevender, and W. D. Oliver, "Impact of ionizing radiation on superconducting qubit coherence," Nature **584**, 551–556 (2020).
[12] M. McEwen, L. Faoro, K. Arya, A. Dunsworth, T. Huang, S. Kim, B. Burkett, A. Fowler, F. Arute, J. C. Bardin, A. Bengtsson, A. Bilmes, B. B. Buckley, N. Bushnell, Z. Chen, R. Collins, S. Demura, A. R. Derk, C. Erickson, M. Giustina, S. D. Harrington, S. Hong, E. Jeffrey, J. Kelly, P. V. Klimov, F. Kostritsa, P. Laptev, A. Locharla, X. Mi, K. C. Miao, S. Montazeri, J. Mutus, O. Naaman, M. Neeley, C. Neill, A. Opremcak, C. Quintana, N. Redd, P. Roushan, D. Sank, K. J. Satzinger, V. Shvarts, T. White, Z. J. Yao, P. Yeh, J. Yoo, Y. Chen, V. Smelyanskiy, J. M. Martinis, H. Neven, A. Megrant, L. Ioffe, and R. Barends, "Resolving catastrophic error bursts from cosmic rays in large arrays of superconducting qubits," arXiv:2104.05219 (2021).
[13] R. Barends, J. Wenner, M. Lenander, Y. Chen, R. C. Bialczak, J. Kelly, E. Lucero, P. O'Malley, M. Mariantoni, D. Sank, H. Wang, T. C. White, Y. Yin, J. Zhao, A. N. Cleland, J. M. Martinis, and J. J. Baselmans, "Minimizing quasiparticle generation from stray infrared light in superconducting quantum circuits," Appl. Phys. Lett. **99**, 113507 (2011).
[14] L. Cardani, F. Valenti, N. Casali, G. Catelani, T. Charpentier, M. Clemenza, I. Colantoni, A. Cruciani, G. D'Imperio, L. Gironi, L. Grünhaupt, D. Gusenkova, F. Henriques, M. Lagoin, M. Martinez, G. Pettinari, C. Rusconi, O. Sander, C. Tomei, A. V. Ustinov, M. Weber, W. Wernsdorfer, M. Vignati, S. Pirro, and I. M. Pop, "Reducing the impact of radioactivity on quantum circuits in a deep-underground facility," Nat. Commun. **12**, 2733 (2021).
[15] C. D. Wilen, S. Abdullah, N. A. Kurinsky, C. Stanford, L. Cardani, G. D'Imperio, C. Tomei, L. Faoro, L. B. Ioffe, C. H. Liu, A. Opremcak, B. G. Christensen, J. L. DuBois, and R. McDermott, "Correlated charge noise and relaxation errors in superconducting qubits," Nature **594**, 369–373 (2021).
[16] C. Kurter, C. E. Murray, R. T. Gordon, B. B. Wymore, M. Sandberg, R. M. Shelby, A. Eddins, V. P. Adiga, A. D. K. Finck, E. Rivera, A. A. Stabile, B. Trimm, B. Wacaser, K. Balakrishnan, A. Pyzyna, J. Sleight, M. Steffen, and K. Rodbell, "Quasiparticle tunneling as a probe of Josephson junction quality and capacitor material in superconducting qubits," arXiv:2106.11488 (2021).
[17] L. Sun, L. Dicarlo, M. D. Reed, G. Catelani, L. S. Bishop, D. I. Schuster, B. R. Johnson, G. A. Yang, L. Frunzio, L. Glazman, M. H. Devoret, and R. J. Schoelkopf, "Measurements of quasiparticle tunneling dynamics in a band-gap-engineered transmon qubit," Phys. Rev. Lett. **108**, 230509 (2012).
[18] D. Ristè, C. C. Bultink, M. J. Tiggelman, R. N. Schouten, K. W. Lehnert, and L. Dicarlo, "Millisecond charge-parity fluctuations and induced decoherence in a superconducting transmon qubit," Nat. Commun. **4**, 1913 (2013).
[19] K. Serniak, S. Diamond, M. Hays, V. Fatemi, S. Shankar, L. Frunzio, R. J. Schoelkopf, and M. H. Devoret, "Direct dispersive monitoring of charge parity in offset-charge-sensitive transmons," Phys. Rev. Appl. **12**, 014052 (2019).
[20] M. Zgirski, L. Bretheau, Q. Le Masne, H. Pothier, D. Esteve, and C. Urbina, "Evidence for long-lived quasiparticles trapped in superconducting point contacts," Phys. Rev. Lett. **106**, 257003 (2011).
[21] E. M. Levenson-Falk, F. Kos, R. Vijay, L. Glazman, and I. Siddiqi, "Single-quasiparticle trapping in aluminum nanobridge Josephson junctions," Phys. Rev. Lett. **112**, 047002 (2014).
[22] C. Janvier, L. Tosi, L. Bretheau, Ç. Ö. Girit, M. Stern, P. Bertet, P. Joyez, D. Vion, D. Esteve, M. F. Goffman, H. Pothier, and C. Urbina, "Coherent manipulation of Andreev states in superconducting atomic contacts," Science **349**, 1199–1202 (2015).
[23] M. Hays, G. de Lange, K. Serniak, D. J. van Woerkom, D. Bouman, P. Krogstrup, J. Nygård, A. Geresdi, and M. H. Devoret, "Direct microwave measurement of Andreev-bound-state dynamics in a semiconductor-nanowire Josephson junction," Phys. Rev. Lett. **121**, 047001 (2018).
[24] M. Hays, V. Fatemi, K. Serniak, D. Bouman, S. Diamond, G. de Lange, P. Krogstrup, J. Nygård, A. Geresdi, and M. H. Devoret, "Continuous monitoring of a trapped superconducting spin," Nat. Phys. **16**, 1103–1107 (2020).
[25] R.-P. Riwar, A. Hosseinkhani, L. D. Burkhart, Y. Y. Gao, R. J. Schoelkopf, L. I. Glazman, and G. Catelani, "Normal-metal quasiparticle traps for superconducting qubits," Phys. Rev. B **94**, 104516 (2016).
[26] J. M. Martinis, "Saving superconducting quantum processors from decay and correlated errors generated by gamma and cosmic rays," npj Quantum Inf. **7**, 90 (2021).
[27] U. Patel, I. V. Pechenezhskiy, B. L. T. Plourde, M. G. Vavilov, and R. McDermott, "Phonon-mediated quasiparticle poisoning of superconducting microwave resonators," Phys. Rev. B **96**, 220501 (2017).
[28] A. F. Andreev, "Thermal conductivity of the intermediate state in superconductors," J. Exp. Theor. Phys. **19**, 1228 (1964).
[29] R. Vijay, J. D. Sau, M. L. Cohen, and I. Siddiqi, "Optimizing anharmonicity in nanoscale weak link Josephson junction oscillators," Phys. Rev. Lett. **103**, 087003 (2009).
[30] R. Vijay, E. M. Levenson-Falk, D. H. Slichter, and I. Siddiqi, "Approaching ideal weak link behavior with three dimensional aluminum nanobridges," Appl. Phys. Lett. **96**, 223112 (2010).
[31] E. M. Levenson-Falk, R. Vijay, and I. Siddiqi, "Nonlinear microwave response of aluminum weak-link Josephson oscillators," Appl. Phys. Lett. **98**, 123115 (2011).
[32] O. Dorokhov, "Transmission coefficient and the localization length of an electron in N bound disordered chains," JETP Lett. **36**, 259 (1982).
[33] C. Macklin, K. O'brien, D. Hover, M. Schwartz, V. Bolkhovsky, X. Zhang, W. Oliver, and I. Siddiqi, "A near–quantum-limited josephson traveling-wave parametric amplifier," Science **350**, 307–310 (2015).
[34] F. Pedregosa, G. Varoquaux, A. Gramfort, V. Michel, B. Thirion, O. Grisel, M. Blondel, P. Prettenhofer, R. Weiss, V. Dubourg, J. Vanderplas, A. Passos, D. Cournapeau, M. Brucher, M. Perrot, and E. Duchesnay, "Scikit-learn: Machine learning in Python," J. Mach. Learn. Res. **12**, 2825–2830 (2011).
[35] O. Naaman and J. Aumentado, "Poisson transition rates from time-domain measurements with a finite bandwidth," Phys. Rev. Lett. **96**, 100201 (2006).